Vol. 23, No. 2(2024) IE24235
Revista Mexicana de Ingeniería Química

Soft chemistry synthesis of size-controlled ZnO nanostructures as photoanode for dye-sensitized solar cell

Síntesis de nanoestructuras de ZnO de tamaño contolado por el proceso de química blanda como fotoánodos para la celda solar de tercera generación

R. García-Molina[1], G.G. Suárez-Velázquez[2*], W. J. Pech-Rodríguez[1], L.C. Ordóñez[3], P. C. Melendez-Gonzalez[4], N.M. Sánchez-Padilla[1], D. González-Quijano[5]

[1]*Universidad Politécnica de Victoria, Departamento de maestría en Ingeniería, Parque Científico y Tecnológico de Tamaulipas, Ciudad Victoria, Tamaulipas 87138, México.*

[2]*Universidad Politécnica de Altamira, Departamento de Ingeniería en energía, Nuevo Libramiento Altamira Km. 3, Santa Amalia, Altamira, Tamaulipas 89602, México.*

[3]*Centro de Investigación Científica de Yucatán, Unidad de Energía Renovable, Yucatán 97302, México.*

[4]*Cinvestav Unidad Saltillo, Unidad de Nanotecnología, Av. Industria Metalúrgica 1062, Parque Industrial Ramos Arizpe, Ramos Arizpe, Coahuila, 25900, México.*

[5]*Centro de Ciencias de la Ingeniería, Universidad Autónoma de Aguascalientes Campus Sur, Av. Prol. Mahatma Gandhi 6601, Aguascalientes, 20340, México.*

Received: January 9, 2024; Accepted: February 16, 2024

Abstract

This study focuses on the systematic soft chemistry synthesis of ZnO nanoparticles as a photoanode for dye-sensitized solar cells. A microwave-assisted heated polyol route was used to dissociate zinc chloride ($ZnCl_2$) in the presence of different NaOH concentrations and under low water concentrations. The obtained nanomaterial was examined by Fourier transform infrared (FTIR) spectroscopy, X-ray diffraction (XRD), Raman spectroscopy and Scanning Electron Microscopy (SEM). The results confirmed O and Zn bond formation in the fresh material. The anode photocatalytic activity was evaluated in a dye-sensitized solar cell fabricated by electrophoretic deposition. The I-V curve of the as-prepared cell anodes reveals that NaOH high concentration improves the current densities resulting in better electrical efficiencies. The photoluminescence measurements indicate that the high NaOH concentration-prepared sample has significant emissions in the visible region. Dislocation density calculations from XRD data indicate that ZnO samples prepared with high NaOH concentrations have more crystallographic defects like oxygen vacancies or interstitial Zn. Similarly, changes in the E_2 (high) phonon Raman mode intensity in ZnO samples suggest that oxygen vacancy formation is favored at high NaOH concentrations. This study demonstrated a fast synthesis of ZnO nanoparticles with photocatalytic properties in developing materials with sensitive defect-related properties for solar cell applications.

Keywords: soft chemical synthesis, nanoparticles, photocatalysts, oxygen vacancy, solar cell.

Resumen

Este estudio se centra en la síntesis sistemática de química blanda de nanopartículas de ZnO como fotoánodo para celdas solares sensibilizadas con colorante. Se utilizó una ruta de poliol asistida por microondas para disociar el cloruro de zinc ($ZnCl_2$) en presencia de diferentes concentraciones de NaOH y bajas concentraciones de agua. El nanomaterial obtenido se examinó mediante espectroscopia infrarroja por transformada de Fourier (FTIR), difracción de rayos-X (XRD), espectroscopia Raman y Microscopia Electrónica de Barrido (SEM). Los resultados confirmaron la formación de enlaces O y Zn en el material. La actividad fotocatalítica del ánodo se evaluó en una celda solar sensibilizada con colorante fabricada mediante deposición electroforética. La curva I-V de los ánodos de las celdas preparadas revela que la alta concentración de NaOH mejora las densidades de corriente, lo que resulta en mejores eficiencias eléctricas. Las mediciones de fotoluminiscencia indican que la muestra preparada con alta concentración de NaOH tiene emisiones significativas en la región de luz visible. Los cálculos de densidad de dislocaciones a partir de datos de XRD indican que las muestras de ZnO preparadas con altas concentraciones de NaOH tienen más defectos cristalográficos como vacancias de oxígeno o Zn intersticial. Similarmente, los cambios en la intensidad del modo Raman del fonón E_2 (alto) en muestras de ZnO sugieren que la formación de vacancias de oxígeno se ve favorecida a altas concentraciones de NaOH. Este estudio demostró una rápida síntesis de nanopartículas de ZnO con propiedades fotocatalíticas para desarrollo de materiales con propiedades sensibles relacionadas con defectos para aplicaciones de celdas solares.

Palabras clave: síntesis química suave, nanopartículas, fotocatálisis, vacancia de oxígeno, celda solar.

*Corresponding author. *E-mail*: gladis.suarez@upalt.edu.mx;
https://doi.org/10.24275/rmiq/IE24235
ISSN:1665-2738, *issn-e*: 2395-8472

1 Introduction

Nowadays, great interest has been devoted to understanding the nature and properties of micro- or nanostructures to be applied to develop sustainable technologies for energy generation (Jayaprabakar *et al*., 2024; Rahman, Bashar, Rahman, & Chowdhury, 2023). To this end, many chemical elements have been used to form functional compounds with unique characteristics that can be used in devices such as solar cells, fuel cells, batteries, and so on (Bogomolov & Ein-Eli, 2023; Prajapat *et al*., 2023; Shah, Lund, & Zhu, 2023).

Over the last decades, semiconducting metal oxide materials have gained considerable attention due to their optical, electrical and physicochemical properties (Xingtai Chen, Liu, Li, & Yin, 2023; Oxandale, Reinke, Das, & El-Kady, 2023; Yang *et al*., 2023). The scientific community has shown great interest in boosting their physical and chemical properties to improve light harvesting in optoelectronic applications (Dou *et al*., 2011; Ntwaeaborwa, Mofokeng, Kumar, & Kroon, 2017). In addition, ZnO semiconducting material has been extensively used as a photoanode in dye-sensitized solar cells (DSSCs) due to their high electrical conductivity, high electron mobility, photostability and wide bandgap that improve the electronic transport (Arjunan & Senthil, 2013; haq *et al*., 2023; Jagadeesh, Veerappan, Devi, Unni, & Soman, 2023; Khan, Ansari, & Kazmi, 2022; Nandi & Das, 2022). As reported elsewhere, the main problem in ZnO-based semiconductors is the suppressed electron transport due to the fast recombination of the electron-hole pairs (Vivek, Preethi, & Babu, 2022). In this concern, many attempts have been made to reduce the recombination probability by changing the ZnO structure, such as incorporating crystal defects or replacing Zn with another ion (Ntwaeaborwa *et al*., 2017). It is widely accepted that the synthesis method plays a crucial role in the intrinsic properties of ZnO. Certain processes of synthesis are capable of tuning the intrinsic ZnO properties. Nevertheless, others produce unreacted or unstable materials with limited optical and electrical properties (B. Du *et al*., 2021; Sufyan, Mehmood, Qayyum Gill, Nazar, & Ul Haq Khan, 2021; Yao *et al*., 2015). In this regard, many efforts have been made to explore novel, cost-effective, and green synthesis processes of ZnO nanoparticles with suitable photocatalytic activities (Ragavendran *et al*., 2023; Taglieri *et al*., 2023). Nonetheless, synthesis parameters such as time, temperature, chemical concentration, pH and pressure have been used to tune the size and morphology of ZnO nanoparticles to improve their luminescence efficiency. Particle size and the presence of intrinsic defects such as oxygen vacancies and metal-oxygen bond length modify the physical properties of this semiconducting material (Mabate, Maqunga, Ntshibongo, Maumela, & Bingwa, 2023). For instance, the emission band of ZnO nanoparticles in the visible range is defined as a complex process where deep trap states are produced due to crystallographic defects such as oxygen or zinc vacancies or oxygen or Zn interstitial sites (Vicencio Garrido, Portillo Araiza, Chavez Portillo, Portillo, & Lozano Espinoza, 2023). One important defect in ZnO^- based materials is oxygen vacancy. This defect could be doubly ionized to form Vo^{2+}, after the acceptance of two valence band holes, which provokes lattice distortion contributing to the enhancement of optical properties (Cooper, Ling, Longo, Li, & Zhang, 2012).

For these reasons, innovative strategies have been proposed to engineer ZnO nanostructures with enhanced photocatalytic properties. Supin and co-workers studied the effect of *Lepidagathis ananthapuramensis* leaf extract concentration on the photocatalytic activity of ZnO nanoparticles. They reported that leaf extract concentration along with calcination parameters activation introduces structural defects (Supin, Parvathy Namboothiri, & Vasundhara, 2023). The defects were estimated by the change in the band gap and the decrease in X-ray Diffraction (XRD) intensity. Additionally, the authors discovered that the incorporation of defects altered the photocatalytic efficiency for methylene blue degradation, attributed to the introduced defect levels in the conduction and valence bands. Vertical ZnO nanorods have also been successfully synthesized using a biopolymer gelation agent (El Faroudi *et al*., 2023). In the case of ZnO^- chitosan, the structure exhibited adsorption in both the visible and UV range, attributed to intrinsic defects in ZnO.

Lizama *et al*. studied the production of ZnO nanomaterials with different morphologies by implementing a sonochemical approach (Lizama-Tzec *et al*., 2016). The synthesis was achieved by mixing zinc acetate dehydrate with deionized water and ammonium hydroxide. The solution was summited to ultrasonic agitation for 3 h under an argon atmosphere, and the final slurry was recovered and dried at 70 °C for 6 h. They found that the pH of the solution changes the morphology and the preferential orientation of ZnO nanoparticles. The measured I-V curve showed an efficiency of 0.43 % for the material synthesized at 10 pH with a short circuit current density (J_{sc}) of 1.16 mA cm^{-2} and an open circuit potential (VOC) of 0.7 V.

Chen and coworkers reported nanoflower-like ZnO materials prepared by hydrothermal process (Xiaobo Chen, Tang, & Liu, 2017). The route consisted of mixing $ZnCl_2$ and NaOH in pure water and then transferring them to an autoclave reactor at 80 °C for 0.5 h. Finally, the solid

was dried at 50 °C for 3 h. The synthesized material showed enhanced activity for UV/Vis absorption, which leads to more photogenerated charge carriers. The electrochemical impedance spectroscopy (EIS) revealed that ZnO nanoflower has better charge transport properties compared with ZnO nanoparticles. In another pertinent study conducted by Jung, sub-micrometre ZnO spheres were also fabricated by the hydrothermal method (Jung, 2017). The material was obtained from a methanolic solution of zinc acetate dehydrate, mixed with tetrabutylammonium hydroxide and transferred to a titanium autoclave at 60 °C for 24 h. Subsequently, the recovered solid was annealed at 500 °C for 30 min. The electrical characterizations of the prepared DSSC indicated that the sub-micrometer ZnO spheres reached an efficiency of 6.01 % at a J_{sc} of 12.05 mA cm^{-2}. The EIS measurements showed that the better performance of ZnO spheres was due to the increase in electron lifetime and faster electron transfer. As can be seen, all the aforementioned processes are time-demanding and associated either with high temperatures or the use of chemical reagents that are not environmentally friendly.

In this research, the assisted intermittent microwave polyol process is proposed to prepare in a short reduction time (2 min) ZnO nanoparticles with photocatalytic properties. The physicochemical properties of ZnO were tuned by controlling the NaOH concentration in the synthesis media. The obtained ZnO materials were used as photoanodes for DSSC and were characterized by conducting electrical measurements. This innovative methodology enables the preparation of ZnO nanoparticles with intrinsic defects in a very short reduction time, just 2 min, and at low temperatures.

2 Materials and methods

2.1 Materials

ZnO nanoparticles were synthesized with the following raw materials: zinc chloride ($ZnCl_2$, 98%) ethylene glycol ($C_2H_6O_2$, 98 %), sodium hydroxide (NaOH, 97%) and deionized water (H_2O, 99 %) all purchased from Jalmek, México. All the chemical reagents were analytical grade and used as received.

Photoanode and the DSSC were fabricated by using 2-propanol (99.5 %, Sigma-Aldrich), magnesium nitrate hexa-hydrated ($Mg(NO_3)_2$ $6H_2O$, 99.99%, Sigma-Aldrich), ruthenium complex (N719, Solaronix), Surlylin® film (Solaronix), platinum solution (Platisol®, Solaronix), F-doped SnO2 conductive glass substrate (Solaronix), and Iodolyte® solution (HI-30, Solaronix).

2.2 Synthesis of ZnO nanoparticles

The photocatalytic material was synthesized by the assisted microwave heating polyol process as follows: in a round bottom flask, the desired amount of zinc chloride was dispersed in ethylene glycol solution with a relation of 24.5:1 (mg:mL) by using an ultrasonic bath. Then, the sample was maintained under vigorous stirring, and 2 mL of deionized water was added to the obtained solution. In order to study the effect of NaOH in the formation of ZnO nanoparticles, three different volumes (2 mL, 3 mL and 4 mL) of 1.5 mol L^{-1} NaOH solution were added to the synthesis media. Then, the colloidal mixture was placed in a modified domestic microwave oven (Daewoo, 1500 W) with a reflux system and was heated for a short period of 2 min, reaching a temperature of 196 °C. Finally, the obtained slurry was washed with copious deionized water in a vacuum filtering system and dried at 100 °C for 10 min.

2.3 Photoanode and DSSC fabrication

The photoanode for the DSSC was fabricated, as is reported in (Zapata-Cruz *et al*., 2019). Briefly, the as-synthesized ZnO nanoparticles were dispersed in 2-propanol for 10 min, and then 0.01 mg mL^{-1} of $Mg(NO_3)_2$ $6H_2O$ was added as a charging agent under sonification for 10 min. The obtained mixture was transferred to an electrochemical cell with a 316 L stainless steel counter electrode. The working electrode was a conductive glass substrate with an exposed area of 0.16 cm^{-2}. The electrophoretic deposition (EPD) was conducted by applying 40 V with a Chroma 61604 power source for 4 min. Then, a new mixture of ZnO was used to obtain a second laminated layer. The obtained photoanode was thermally treated at 400 °C for 1 h and then was sensitized by immersing in a 0.35 m mol L^{-1} N719 ethanolic solution for 3 h. The DSSC cathode was fabricated by transferring a Platisol® solution onto the conductive glass substrate. The chemical reduction of Pt was accomplished by heating the sample at 450 °C for 5 min in air. Finally, the photoanode and the cathode were assembled in a typical sandwich setup using thermoplastic sealing and heated at 160 °C for 3 min. The electrolyte solution was injected through the counter electrode small hole.

2.4 Physicochemical characterization

The chemical bonds in the ZnO nanomaterial were studied by performing Fourier Transform Infrared Spectroscopy (FTIR) measurements in a WQF-510A (Rayleigh instrument) spectrometer using compressed KBr disks. The test was conducted in transmittance mode with a resolution of 4 cm^{-1}. The structure of the obtained ZnO materials was investigated by

X-ray Diffraction (XRD) in a Bruker D2 phaser 2nd generation in a 10-100 (2θ) range with a step scan of 0.01° per 0.4 s. The morphology of the as-prepared ZnO was studied by Scanning Electron Microscopy (SEM, JEOL-JSM-6360). Raman spectra were recorded in a Thermo Scientific DXR2 using a 633 nm Ar ion laser at 10 mW and resolution of 2 cm^{-1}, in the 100 to 1200 cm^{-1} range. The photoluminescence spectra of the ZnO were recorded using Thorlab CCS200 equipment at room temperature. To simulate the operating conditions of the semiconductor in a dye-sensitized solar cell, the ZnO nanoparticles were suspended in an ethanol-ruthenium solution, 8 mL alcohol and 690 μL of 0.35 mmol L^{-1} N719.

2.5 *Electrical characterization*

The electrical parameters of the fabricated DSSC were obtained by using a potentiostat (Gill AC-ACM Instruments Ltd) in a two-electrode configuration. The Linear Sweep Voltammetry (LSV) was measured from the open circuit potential to 0 volts at a scan rate of 5 mVs^{-1}. The DSSC with an active area of 0.16 cm^{-2} was exposed to simulated sunlight AM1.5 (100 mW cm^{-2}, SunLite 11002).

3 Results and discussion

3.1 *DSSC electrical performance*

Figure 1 displays the current density-voltage plot for the fabricated dye-sensitized solar cells using the as-synthesized ZnO compound. It can be inferred that NaOH concentration plays a crucial role in the final electrical efficiency. All samples exhibit a nearly identical open circuit potential, approximately 0.6 V. However, among them, the ZnO-4 mL sample delivers the highest J_{sc}, close to 13 mA cm^{-2}.

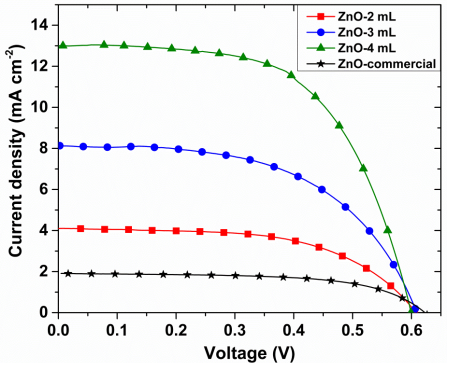

Figure 1. Photocurrent plot of the DSSC fabricated with the electrophoretic deposition of ZnO nanoparticles.

Table 1. Determined electrical parameters of the assembled DSSC using the as-prepared ZnO and the DSSC with commercial ZnO.

Sample	V_{OC} (V)	Jsc (mA cm^{-2})	Fill factor	Efficiency (%)
ZnO-commercial	0.62	1.91	0.60	0.72
ZnO-2mL	0.60	4.12	0.57	1.41
ZnO-3mL	0.6	8.13	0.54	2.7
ZnO-4mL	0.59	13.04	0.58	4.6

Conversely, the sample with the lowest NaOH concentration displayed decreased efficiency. Table 1 provides a summary of the electrical parameters determined for all samples. Notably, the ZnO-4 mL sample exhibited the highest electrical efficiency, 4.6 %, outperforming commercial ZnO, which displayed the lowest, 0.72 %. The results are surprising and suggest that ZnO-4 mL (with a high NaOH concentration) is promising as an anode for DSSC when compared to other materials documented in the literature (Atanacio-Sánchez *et al*., 2020; Sehgal & Narula, 2021; Sufyan *et al*., 2021).

As reported elsewhere, the photocurrent densities in a dye sensitized solar cell highly depend on morphology, particle size, the thickness of the deposited layer and intrinsic defects in the semiconductor that change the electron recombination rate and the visible light adsorption (Velazquez-Gonzalez, Armendariz-Mireles, Pech-Rodriguez, González-Quijano, & Rocha-Rangel, 2019; Zapata-Cruz *et al*., 2019). In this context, additional material characterization was performed to gain deeper insights into the impact of NaOH concentration on the resulting current density of the fabricated DSSC.

3.2 *Physicochemical characterization*

Figure 2 shows the FTIR spectra of the ZnO sample. They present broadband between 3000 and 3681 cm^{-1}, corresponding to the stretching vibrations of different hydroxyl groups on the ZnO surface. The peak at 1635 cm^{-1} corresponds to the stretching vibrations of Zn-O. At 1423 cm^{-1} and 1051 cm^{-1} the C=O and C-O stretching vibrations were observed. The band at 902 cm^{-1} is associated with the formation of Zn with tetrahedral coordination. The peak at 715 cm^{-1} is related to the ZnO nanoparticles (Rana, 2017). The band at 439 cm^{-1}, is attributed to the Zn-O stretching vibration corresponding to the ZnO lattice (Quek, Sin, Lam, Mohamed, & Zeng, 2020; Wallace, Brown, Brydson, Wegner, & Milne, 2013). All samples show at 2353 cm^{-1} the band weakly bonded CO2 to the ZnO surface (Ramzan Parra & Haque, 2015).

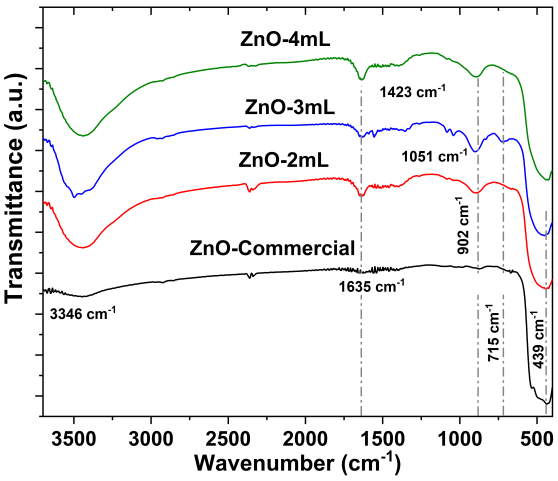

Figure 2. FTIR spectra for the as-synthesized ZnO compounds.

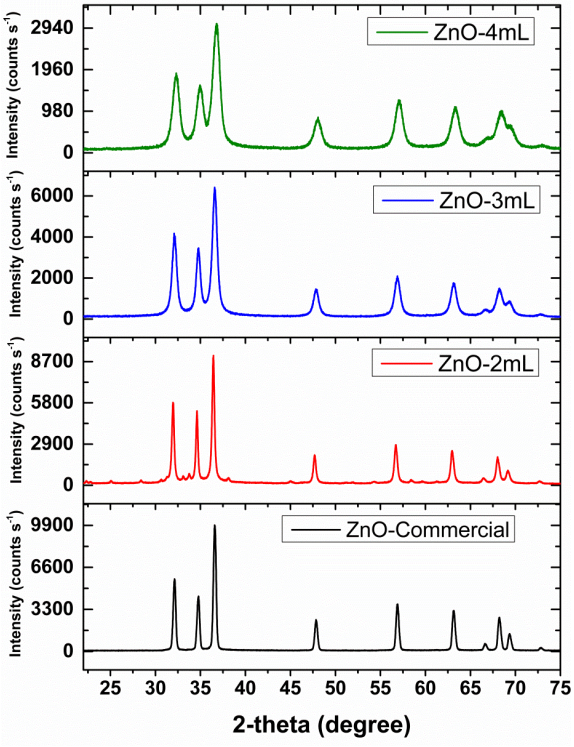

Figure 3. XRD patterns for the commercial ZnO and the ZnO prepared in this work.

XRD powder measurements were achieved to determine the crystallographic structure from the as-synthesized ZnO materials with different NaOH concentrations. Figure 3 displays the X-ray diffractograms for the commercial and the synthesized ZnO compound. The synthesized material was polycrystalline and was well indexed with the JCPDS card No. 36-1451, corresponding to the hexagonal wurtzite structure of ZnO. The main reflection peaks were observed close to 32°, 34.6°, 36.5°, .47.8°, 56.8°, 63.0°, 66.6°, 68°, 69.3°, and 72.8° 2-theta corresponding to the planes (100), (002), (101), (102), (110), (103), (200), (112), (201), and (004), respectively. No other relevant peaks were detected, which indicates the successful ZnO formation from zinc chloride and NaOH as raw material through the microwave-assisted polyol reduction method at low temperatures and short synthesis time. An intriguing finding is that the as-synthesized ZnO materials have slightly lower reflection peaks (in counts) as the concentration of NaOH increases. This phenomenon could be attributed to a reduced degree of crystallinity or a decrease in crystallite size. To investigate further, the average crystallite size was determined using the Debye-Scherrer equation.

Table 2 summarizes the calculated crystallite size for each sample. ZnO-4 mL compound has the smallest size, 9.34 nm, and it increases as the NaOH in the formulation decreases. Therefore, as stated before, the low intensities in the ZnO nanomaterials are due to the small crystallite size. Compared to the commercial one, the as-synthesized ZnO reflections are shifted to a higher Bragg's angle, in agreement with a decrease in the lattice parameters calculated considering a hexagonal structure and using the following equation:

$$\sin^2\theta = \frac{\lambda^2}{4}\left[\frac{4}{3}\left(\frac{h^2+hk+k^2}{a^2}\right)\right] \quad (1)$$

where λ is the radiation wavelength (1.5406 Å), *hkl* are the index at the specific plane, and a is the lattice parameter (Table 2). The NaOH concentration affected the lattice parameters for all as-synthesized ZnO nanomaterial. It has been reported that the decrease in lattice parameters in ZnO is due to the incorporation of defects such as oxygen vacancies or Zn deficiencies (X. Li, Wang, Liu, Jiang, & Zhu, 2012). For example, the research group of Chen reported a decrease in peak intensities of milled ZnO samples compared with the pristine ZnO. This change in intensity was attributed to the formation of defects during the ball-milling process (D. Chen *et al.*, 2014).

The theoretical density of the samples was calculated according to our previously reported work (Velazquez-Gonzalez *et al.*, 2019) and is listed in Table 1. The ZnO surface area (SA) was determined by the following equation considering spherical nanoparticles:

$$SA = \frac{6\times10^3}{d} \quad (2)$$

where ρ is the theoretical density and d is the crystallite size. ZnO-4mL has the highest surface area compared with the other materials. Therefore, it is important to highlight that ZnO materials with smaller crystallite sizes can enhance the efficiency of sunlight conversion due to the increase in surface area (Wibowo *et al.*, 2020).

It is reported that material vacancies originate from crystal defects. Thus dislocation density (δ) was calculated according to the following equation (Bindu

& Thomas, 2014):

$$\delta = \frac{1}{d^2} \tag{3}$$

From Table 2, it can be observed that ZnO-4 mL has a large dislocation density which implies a higher vacancy density (Bindu & Thomas, 2014). Meanwhile, the bond length between Zn and O was determined as follows:

$$L = \sqrt{\frac{a^2}{3} + \left(\frac{1}{2} - \frac{a^2}{3c^2} + 0.25\right)^2 c^2} \tag{4}$$

Along with dislocation density formation, a change in the Zn-O bond length is observed. Also, the ZnO-4 mL sample has the lowest Zn-O bond length suggesting changes in energies at electronic levels that could affect its photocatalytic activity and shorten the charge carriers' transport distance (Bindu & Thomas, 2014).

Figure 4 presents the SEM micrographs of the as-prepared ZnO-4 mL compound under two different magnifications. It should be noted that the material is composed of agglomerated nanoparticles forming clusters below 1.9 μm in length, see Figure 4-a. To gain deeper insight into the morphology of the sample, high magnification was employed, Figure 4-b, revealing that the observed clusters are comprised of small nanoparticles. Specifically, the enclosed small red circles highlight agglomerated nanoparticles with dimensions below 40 nm. The SEM results support the data extracted from the XRD patterns where a crystallite size of approximately 9.4 nm was calculated.

From XRD results it is deduced that the as-synthesized ZnO nanoparticles have a hexagonal structure with space group P63mc and have two sublattices of Zn^{2+} and O^{2-} (Gaikwad *et al.*, 2014; Yousif, Mahdi, & Alshamsi, 2021). Theoretically, the optical phonon in this space group is represented as:

$$\Gamma_{opt} = A_1 + E_1 + 2E_2 + 2B_1 \tag{5}$$

Where A_1, E_1 and E_2 are the active modes, under Raman measurement, and B_1 are silent modes. The E_2 mode is non-polar and is presented as E_2 (high) and E_2 (low). According to this information, the 437 cm^{-1} band (see Figure 5) is due to the high E_2 mode, a characteristic of the oxygen atoms' vibrations in the ZnO wurtzite structure (Li *et al.*, 2007). It has already been reported that crystallographic defects, such as oxygen vacancies, decrease the E_2 (high) intensity due to loss in crystallinity quality (Daiko *et al.*, 2017).

The band at 332 cm^{-1} is assigned to the second-order boundary phonons. The peak at 378 cm^{-1} corresponds to order-disorder in lattice A_1(TO) mode (Dong, Zhang, Deng, You, & Qian, 2006). The broad peak close to 580 cm^{-1} is a weak band E1 mode (LO) for the ZnO structures due to oxygen deficiency or vacancy (Y.-P. Du, Zhang, Sun, & Yan, 2008). At lower frequencies, it is observed a broad peak at 1100 cm^{-1} assigned to the second-order $2A_1$LO phonon

Table 2. XRD calculated parameters for ZnO nanoparticles.

Sample	Average crystallite size (nm)	Lattice constant (Å)	Theoretical density (g·cm^{-3})	Superficial area (m^2·g^{-1})	Dislocation density (nm^{-2})	Zn-O bond length (Å)
ZnO-commercial	24.3	a=b=3.23650 c=5.16019	5.772	43.3	0.00168	1.9667
ZnO-2mL	25.1	a=b=3.24583 c=5.18245	5.714	42.0	0.00158	1.9732
ZnO-3mL	12.5	a=b=3.23689 c=5.15835	5.773	83.9	0.00630	1.9666
ZnO-4mL	9.34	a=b=3.22732 c=5.13047	5.839	113.1	0.01145	1.9593

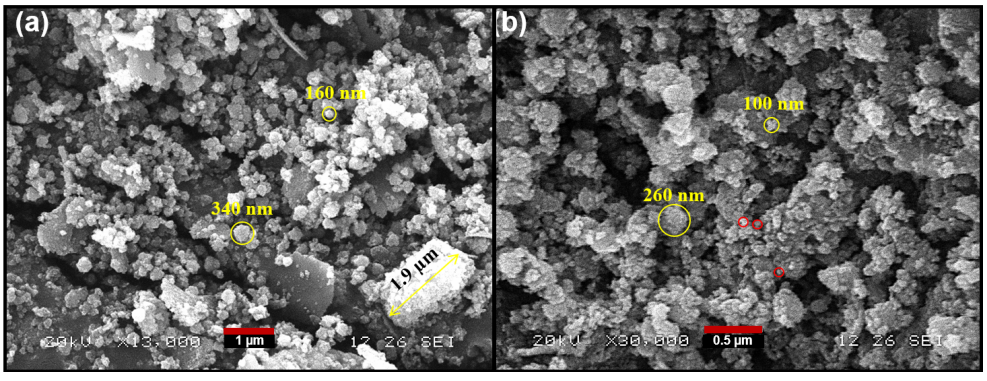

Figure 4. SEM image of the ZnO-4 mL at different magnifications. a) 13,000x; b) 30,000x.

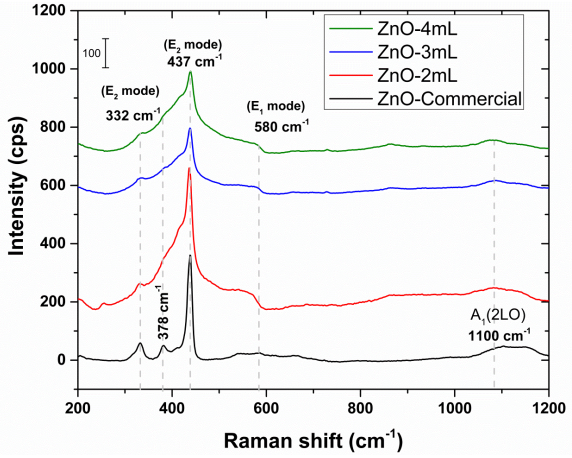

Figure 5. Raman spectra of the bulk ZnO nanoparticles.

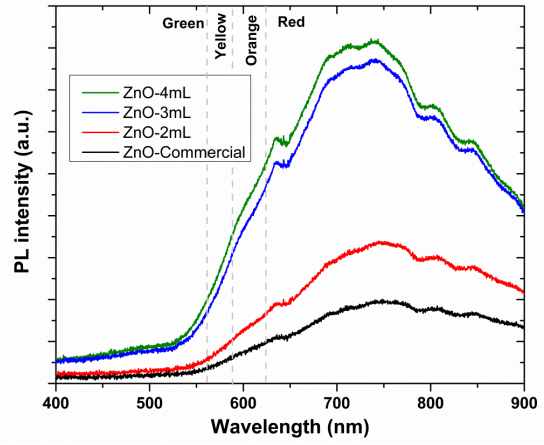

Figure 6 PL spectra in ethanolic solution for the ZnO compounds sensitized with N719.

It is worth mentioning that the E_2 (high mode-437 cm^{-1}) peak is less intense in ZnO-3mL and ZnO-4mL, in other words, the samples with high NaOH concentration. As stated before, these two samples have lower lattice parameters, and this effect results from crystallographic defects such as oxygen or zinc vacancies. Because the E_2 mode results from oxygen vibration in the ZnO structure, the lower intensities in this peak suggest that the defect is due to oxygen vacancies. This assumption was studied in detail by the research work of Fukushime where they proposed a correlation between the E_2 (high) phonon mode and the number of oxygen vacancies in the ZnO sample. They found that the Raman intensity decreases linearly as the oxygen vacancies increase (H. Fukushima *et al*., 2015; Hiroaki Fukushima, Uchida, Funakubo, Katoda, & Nishida, 2017). Therefore, considering the values of dislocation densities (determined by XRD analysis) and the decrease in intensity in the Raman spectra, we concluded that ZnO-3mL and ZnO-4mL have more oxygen vacancies.

3.3 Photoluminescence spectra for ZnO

Figure 6 shows the photoluminescence (PL) spectra recorded at room temperature of the ZnO samples. The PL spectra present an emission band in the visible region, and its intensity is higher as the concentration of NaOH increases. The increase in visible light emission may be because of two reasons. One, from the XRD results, is deduced that crystallite size may be the affected parameter with the NaOH content in the synthesis media. Thus, the increase in emission can be related to the particle size decrease. In this direction, Kumar and coworkers stated that small particle size improves the rate of the surface trapping process, and this fact can be corroborated by the large surface area obtained in ZnO-3mL and ZnO-4mL samples (Kumar, Kumar, Gedanken, & Paik, 2014). The second reason is the smallest lattice parameter (for ZnO-3mL and ZnO-4mL samples) which was attributed to oxygen vacancies presence. The probability of radiative recombination of the photogenerated hole with the electron increases with the oxygen vacancy position, and therefore visible emission is higher (Ntwaeaborwa *et al*., 2017; Raji & Gopchandran, 2017). This phenomenon was also observed by Aggelopoulos who studied mechanically activated ZnO nanoparticles by PL measurements as a tool to estimate oxygen vacancies-related defects. He stated that the weakly visible band for the untreated ZnO was attributed to the presence of low defect concentrations (Aggelopoulos *et al*., 2017).

Table 3 summarizes the characteristics of some novel research with the as-synthesized ZnO-4mL. It stands out that the current density delivered by ZnO-4mL is, in most cases, higher than those reported in the literature. Moreover, it is worth mentioning that we proposed a rapid ZnO synthesis (the reduction of the precursor was achieved in 2 min) by using simple laboratory equipment.

It is important to mention ZnO nanoparticles were not obtained under the experimental conditions when there was no water content in the synthesis solution. However, we observe a high-yield conversion of ZnO when water is added. Based on these observations, we proposed a mechanism for the ZnO formation in the presence of ethylene glycol, water, and NaOH, which is presented in Figure 7.

In the beginning, $ZnCl_2$ was dissociated in ethylene glycol, forming Zn cation. Then, the addition of water and NaOH produces two different processes: first, the formation of $Zn(OH)_2$ species. Second, the same chemical conditions lead to the formation of glycolate, favored in alkaline pH. Once the glycolate and $Zn(OH)_2$ species are formed, the increase in temperature leads to the reduction of the Zn species to ZnO. Some studies suggest that in polyol synthesis the metal-polyolate species strongly favors the chelate formation leading to the formation of nanoparticles (Fiévet *et al*., 2018).

Table 3. Comparison of current density with the last published research works.

Sample	Current density (mA cm^{-2})	Voltage (V)	Sensitizer	Reference
ZnO-4mL	13.0	0.6	N719	This work
ZnO	6.26	0.65	N719	Shashanka, *et al.* (2020)
ZnO	8.05	0.58	N719	Ramya *et al*. (2021)
ZnO rare-earth	9.6	0.5	BMII	Sehgal & Narula (2021)
ZnO:TiO_2	14.2	0.7	N719	Zatirostami (2021)

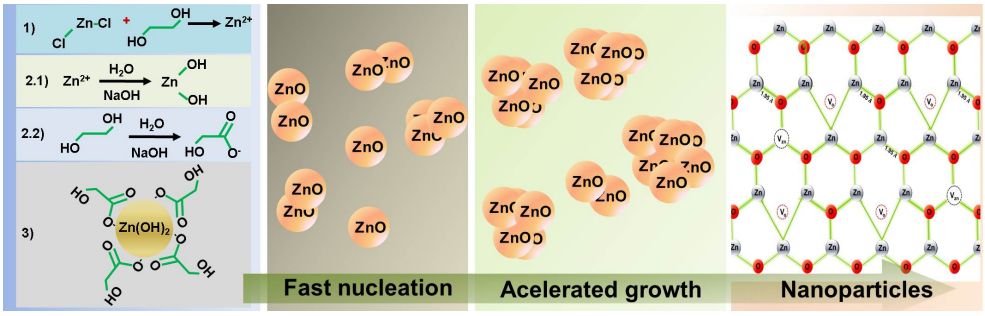

Figure 7. Schematic diagram for the ZnO nanoparticle formation.

3.4 Discussion

From the XRD and Raman spectroscopy results, the role of NaOH concentration in the synthesis solution is likely accelerating the formation of small nuclei centres. Thus, explain the small crystallite size at high NaOH concentration. On the other hand, high NaOH concentration promotes the rapid formation of ZnO due to the improvement of dissolution-precipitation reactions. The accelerated ZnO crystallization, generates high content of oxygen vacancies, as has previously been reported by Wang (Wang *et al*., 2016). Also, microwave irradiation plays a crucial role in the growth of ZnO nanoparticles. It has been reported that microwave-assisted hydrolysis leads to high crystal defects, in ZnO nanoparticles, due to the fast nucleation and crystallization process (Baruah, Mahmood, Myint, Bora, & Dutta, 2010; Mahmood, Baruah, & Dutta, 2011; Ramya, Nideep, Nampoori, & Kailasnath, 2021).

Considering the above-mentioned, the observed high DSSC efficiency is mainly attributed to crystallographic defects in the anode material that promote the generation of the electron pair-hole at low energy levels (Mahmood *et al*., 2011).

Conclusions

This work has demonstrated the feasibility of using the microwave-assisted polyol process to synthesize ZnO nanoparticles. From the results, we can conclude that NaOH concentration is a key parameter of the synthesis process because it accelerates the ZnO formation allowing the creation of oxygen vacancies. Furthermore, the electrical performance of the ZnO-based dye-sensitized solar cell has a severe dependence on NaOH concentration that was attributed to the enhancement in charge generation processes. Therefore, it can be deduced that the optical, physical and chemical properties of ZnO compounds can be tuned by modifying the NaOH concentration. A remaining challenge that must be mentioned is the stability issue of the assembled DSSC. During the measurements, a decrease in the open circuit potential and the current densities was observed. It is well known that factors such as humidity, electrolyte and dye decomposition, as well as detachment of the anode and cathode, are the primary contributors to this phenomenon. Finally, we believe that the proposed green, cost-effective synthesis method can be used for the production of ZnO photocatalysts in a very short time. It may help the study of semiconducting materials in energy storage and generation.

Acknowledgment

We thank the Polytechnic University of Victoria for the facilities and the equipment provided to develop the present research. We acknowledge Martín Baas for support in RAMAN tests and Enrique Escobedo for help with the XRD test. Finally, we thank the National Council of Humanities, Science and Technology (CONAHCYT) grants 253986 and 254667.

References

Aggelopoulos, C. A., Dimitropoulos, M., Govatsi, A., Sygellou, L., Tsakiroglou, C. D., & Yannopoulos, S. N. (2017). Influence of the surface-to-bulk defects ratio of ZnO and TiO_2 on their UV-mediated photocatalytic activity. *Applied Catalysis B: Environmental 205*(1), 292-301. https://doi.org/10.1016/j.apcatb.2016.12.023

Arjunan, T. V., & Senthil, T. S. (2013). Review: Dye sensitised solar cells. *Materials Technology 28*(1-2), 9-14. https://doi.org/10.1179/1753555712Y.0000000040

Atanacio-Sánchez, X., Pech-Rodríguez, W. J., Armendáriz-Mireles, E. N., Castillo-Robles, J. A., Meléndez-González, P. C., & Rocha-Rangel, E. (2020). Improving performance of ZnO flexible dye sensitized solar cell by incorporation of graphene oxide. *Microsystem Technologies 26*(12), 3591-3599. https://doi.org/10.1007/s00542-020-04820-x

Baruah, S., Mahmood, M., Myint, M. T. Z., Bora, T., & Dutta, J. (2010). Enhanced visible light photocatalysis through fast crystallization of zinc oxide nanorods. *Beilstein Journal of Nanotechnology 1*(1), 14-20. https://doi.org/10.3762/bjnano.1.3

Bindu, P., & Thomas, S. (2014). Estimation of lattice strain in ZnO nanoparticles: X-ray peak profile analysis. *Journal of Theoretical and Applied Physics 8*(4), 123-134. https://doi.org/10.1007/s40094-014-0141-9

Bogomolov, K., & Ein-Eli, Y. (2023). Alkaline Ni-Zn rechargeable batteries for sustainable energy storage: Battery components, deterioration mechanisms, and impact of additives. *ChemSusChem*, E202300940. https://doi.org/10.1002/cssc.202300940

Chen, D., Wang, Z., Ren, T., Ding, H., Yao, W., Zong, R., & Zhu, Y. (2014). Influence of defects on the photocatalytic activity of ZnO. *The Journal of Physical Chemistry C 118*(28), 15300-15307. https://doi.org/10.1021/jp5033349

Chen, X., Liu, T., Li, Z., & Yin, X.-T. (2023). Recent developments in metal oxide semiconductors for n-Butanol detection. *Materials Today Chemistry 33*, 101690. https://doi.org/10.1016/j.mtchem.2023.101690

Chen, X., Tang, Y., & Liu, W. (2017). Efficient dye-sensitized solar cells based on nanoflower-like ZnO photoelectrode. *Molecules 22*(8), 1284. http://www.mdpi.com/1420-3049/22/8/1284

Cooper, J. K., Ling, Y., Longo, C., Li, Y., & Zhang, J. Z. (2012). Effects of hydrogen treatment and air annealing on ultrafast charge carrier dynamics in ZnO nanowires under *in situ* photoelectrochemical conditions. *The Journal of Physical Chemistry C 116*(33), 17360-17368. https://doi.org/10.1021/jp304428t

Daiko, Y., Schmidt, J., Kawamura, G., Romeis, S., Segets, D., Iwamoto, Y., & Peukert, W. (2017). Mechanochemically induced sulfur doping in ZnO via oxygen vacancy formation. *Physical Chemistry Chemical Physics 19*(21), 13838-13845. http://dx.doi.org/10.1039/C7CP01489A

Dong, Z. W., Zhang, C. F., Deng, H., You, G. J., & Qian, S. X. (2006). Raman spectra of single micrometer-sized tubular ZnO. *Materials Chemistry and Physics 99*(1), 160-163. https://doi.org/10.1016/j.matchemphys.2005.10.005

Dou, X., Sabba, D., Mathews, N., Wong, L. H., Lam, Y. M., & Mhaisalkar, S. (2011). Hydrothermal synthesis of high electron mobility Zn-doped SnO_2 nanoflowers as photoanode material for efficient dye-sensitized solar cells. *Chemistry of Materials 23*(17), 3938-3945. https://doi.org/10.1021/cm201366z

Du, B., Yao, Y., Shen, M., Luo, Z., Li, M., & Gao, Q. (2021). Synthesis and photocatalytic activity of dumbbell-like mesoporous ZnO micro-nanomaterials with tetrasulfonatomethyl-n-hexyl calix [4]resorcinarene tetrasodium salt as hard-soft template. *Journal of Physics and Chemistry of Solids 150*(1), 109871. https://doi.org/10.1016/j.jpcs.2020.109871

Du, Y.-P., Zhang, Y.-W., Sun, L.-D., & Yan, C.-H. (2008). Efficient energy transfer in monodisperse Eu-doped ZnO nanocrystals synthesized from metal acetylacetonates in high-boiling solvents. *The Journal of Physical Chemistry C 112*(32), 12234-12241. https://doi.org/10.1021/jp802958x

El Faroudi, L., Saadi, L., Barakat, A., Mansori, M., Abdelouahdi, K., & Solhy, A. (2023). Facile and sustainable synthesis of ZnO nanoparticles: Effect of gelling agents on ZnO shapes and their photocatalytic performance. *ACS Omega 8*(28), 24952-24963. https://doi.org/10.1021/acsomega.3c01491

Fiévet, F., Ammar-Merah, S., Brayner, R., Chau, F., Giraud, M., Mammeri, F., . . . Viau, G. (2018). The polyol process: a unique method for easy access to metal nanoparticles with tailored sizes, shapes and compositions. *Chemical Society Reviews 47*(14), 5187-5233. http://dx.doi.org/10.1039/C7CS00777A

Fukushima, H., Kozu, T., Shima, H., Funakubo, H., Uchida, H., Katoda, T., & Nishida, K. (2015, 24-27 May 2015). Evaluation of oxygen vacancy in ZnO using Raman spectroscopy. Paper presented at the 2015 Joint IEEE International Symposium on the Applications of Ferroelectric (ISAF), International Symposium on Integrated Functionalities (ISIF), and Piezoelectric Force Microscopy Workshop (PFM).

Fukushima, H., Uchida, H., Funakubo, H., Katoda, T., & Nishida, K. (2017). Evaluation of oxygen vacancies in ZnO single crystals and powders by micro-Raman spectroscopy. *Journal of the Ceramic Society of Japan 125*(6), 445-448. https://doi.org/10.2109/jcersj2.16262

Gaikwad, S. S., Gandhi, A. C., Pandit, S. D., Pant, J., Chan, T.-S., Cheng, C.-L., . . . Wu, S. Y. (2014). Oxygen induced strained ZnO nanoparticles: an investigation of Raman scattering and visible photoluminescence. *Journal of Materials Chemistry C 2*(35), 7264-7274. http://dx.doi.org/10.1039/C4TC00566J

Haq, I.-u., Khan, M. I., Irfan, M., Fatima, M., Somaily, H. H., Elqahtani, Z. M., & Alwadai, N. (2023). Increase the current density and reduce the defects of ZnO by modification of the band gap edges with Cu ions implantation for efficient, flexible dye-sensitized solar cells (FDSSCs). *Ceramics International 49*(18), 29622-29629. https://doi.org/10.1016/j.ceramint.2023.06.188

Jagadeesh, A., Veerappan, G., Devi, P. S., Unni, K. N. N., & Soman, S. (2023). Synergetic effect of TiO_2/ZnO bilayer photoanodes realizing exceptionally high VOC for dye-sensitized solar cells under outdoor and indoor illumination. *Journal of Materials Chemistry A 11*(27), 14748-14759. https://doi.org/10.1039/D3TA02698A

Jayaprabakar, J., Sri Hari, N. S., Badreenath, M., Anish, M., Joy, N., Prabhu, A., . . . Kumar, J. A. (2024). Nano materials for green hydrogen production: Technical insights on nano material selection, properties, production routes and commercial applications. *International Journal of Hydrogen Energy 52*, 674-686. https://doi.org/10.1016/j.ijhydene.2023.06.109

Jung, M.-H. (2017). High efficiency dye-sensitized solar cells based on the ZnO nanoparticle aggregation sphere. *Materials Chemistry and Physics 202*(1), 234-244. https://doi.org/10.1016/j.matchemphys.2017.09.034

Khan, S., Ansari, A. J., & Kazmi, S. A. (2022, 24-25 June 2022). ZnO-rGO-Ag Photoanode for Dye-sensitized Solar cells. Paper presented at the 2022 2nd International Conference on Emerging Frontiers in Electrical and Electronic Technologies (ICEFEET).

Kumar, V. B., Kumar, K., Gedanken, A., & Paik, P. (2014). Facile synthesis of self-assembled spherical and mesoporous dandelion capsules of ZnO: efficient carrier for DNA and anti-cancer drugs. *Journal of Materials Chemistry B 2*(25), 3956-3964. http://dx.doi.org/10.1039/C4TB00416G

Li, C., Lv, Y., Guo, L., Xu, H., Ai, X., & Zhang, J. (2007). Raman and excitonic photoluminescence characterizations of ZnO star-shaped nanocrystals. *Journal of Luminescence 122*(1), 415-417. https://doi.org/10.1016/j.jlumin.2006.01.173

Li, X., Wang, Y., Liu, W., Jiang, G., & Zhu, C. (2012). Study of oxygen vacancies' influence on the lattice parameter in ZnO thin film. *Materials Letters 85*(1), 25-28. https://doi.org/10.1016/j.matlet.2012.06.107

Lizama-Tzec, F. I., Garcia-Rodriguez, R., Rodriguez-Gattorno, G., Canto-Aguilar, E. J., Vega-Poot, A. G., Heredia-Cervera, B. E., Villanueva-Cab, J., Morales-Flores, N., Pal, U., Oskam, G. (2016). Influence of morphology on the performance of ZnO-based dye-sensitized solar cells. *RSC Advances 6*(44), 37424-37433. http://dx.doi.org/10.1039/C5RA25618F

Mabate, T. P., Maqunga, N. P., Ntshibongo, S., Maumela, M., & Bingwa, N. (2023). Metal oxides and their roles in heterogeneous catalysis: special emphasis on synthesis protocols, intrinsic properties, and their influence in transfer hydrogenation reactions. *SN Applied Sciences 5*(7), 196. doi: 10.1007/s42452-023-05416-6

Mahmood, M. A., Baruah, S., & Dutta, J. (2011). Enhanced visible light photocatalysis by manganese doping or rapid crystallization with ZnO nanoparticles. *Materials Chemistry and Physics 130*(1), 531-535. https://doi.org/10.1016/j.matchemphys.2011.07.018

Nandi, P., & Das, D. (2022). Morphological variations of ZnO nanostructures and its influence on the photovoltaic performance when used as photoanodes in dye sensitized solar cells. *Solar Energy Materials and Solar Cells 243*, 111811. https://doi.org/10.1016/j.solmat.2022.111811

Ntwaeaborwa, O. M., Mofokeng, S. J., Kumar, V., & Kroon, R. E. (2017). Structural, optical and photoluminescence properties of Eu3+ doped ZnO nanoparticles. *Spectrochimica Acta Part A: Molecular and Biomolecular Spectroscopy 182*(1), 42-49. https://doi.org/10.1016/j.saa.2017.03.067

Oxandale, S. W., Reinke, C., Das, S. R., & El-Kady, I. (2023). Enhanced thermoelectric performance via quantum confinement in a metal oxide semiconductor field effect transistor for thermal management. *Communications Materials 4*(1), 85. https://doi.org/10.1038/s43246-023-00397-w

Prajapat, K., Dhonde, M., Sahu, K., Bhojane, P., Murty, V. V. S., & Shirage, P. M. (2023). The evolution of organic materials for efficient dye-sensitized solar cells. *Journal of Photochemistry and Photobiology C: Photochemistry Reviews 55*, 100586. https://doi.org/10.1016/j.jphotochemrev.2023.100586

Quek, J.-A., Sin, J.-C., Lam, S.-M., Mohamed, A. R., & Zeng, H. (2020). Bioinspired green synthesis of ZnO structures with enhanced visible light photocatalytic activity. *Journal of Materials Science: Materials in Electronics 31*(2), 1144-1158. https://doi.org/10.1007/s10854-019-02626-w

Ragavendran, C., Kamaraj, C., Jothimani, K., Priyadharsan, A., Anand Kumar, D., Natarajan, D., & Malafaia, G. (2023). Eco-friendly approach for ZnO nanoparticles synthesis and evaluation of its possible antimicrobial, larvicidal and photocatalytic applications. *Sustainable Materials and Technologies 36*, e00597. https://doi.org/10.1016/j.susmat.2023.e00597

Rahman, M., Bashar, M. S., Rahman, M. L., & Chowdhury, F. I. (2023). Comprehensive review of micro/nanostructured $ZnSnO_3$: characteristics, synthesis, and diverse applications. *RSC Advances 13*(44), 30798-30837. doi: 10.1039/D3RA05481K

Raji, R., & Gopchandran, K. G. (2017). ZnO nanostructures with tunable visible luminescence: Effects of kinetics of chemical reduction and annealing. *Journal of Science: Advanced Materials and Devices 2*(1), 51-58. https://doi.org/10.1016/j.jsamd.2017.02.002

Ramya, M., Nideep, T. K., Nampoori, V. P. N., & Kailasnath, M. (2021). The impact of ZnO nanoparticle size on the performance of photoanodes in DSSC and QDSSC: a comparative study. *Journal of Materials Science: Materials in Electronics 32*(3), 3167-3179. https://doi.org/10.1007/s10854-020-05065-0

Ramzan Parra, M., & Haque, F. Z. (2015). Optical investigation of various morphologies of ZnO nanostructures prepared by PVP-assisted wet chemical method. *Optics and Spectroscopy 118*(5), 765-772. https://doi.org/10.1134/S0030400X15030182

Rana, S. B. (2017). Influence of CTAB assisted capping on the structural and optical properties of ZnO nanoparticles. *Journal of Materials Science: Materials in Electronics 28*(18), 13787-13796. https://doi.org/10.1007/s10854-017-7224-8

Sehgal, P., & Narula, A. K. (2021). Improved optical, electrochemical and photovoltaic properties of dye-sensitized solar cell composed of rare earth-doped zinc oxide. *Journal of Materials Science: Materials in Electronics 32*(12), 16612-16622. https://doi.org/10.1007/s10854-021-06216-7

Shah, M. A. K. Y., Lund, P. D., & Zhu, B. (2023). Toward next-generation fuel cell materials. *iScience 26*(6), 106869. https://doi.org/10.1016/j.isci.2023.106869

Shashanka, R., Esgin, H., Yilmaz, V. M., & Caglar, Y. (2020). Fabrication and characterization of green synthesized ZnO nanoparticle based dye-sensitized solar cells. *Journal of Science: Advanced Materials and Devices 5*(2), 185-191. https://doi.org/10.1016/j.jsamd.2020.04.005

Sufyan, M., Mehmood, U., Qayyum Gill, Y., Nazar, R., & Ul Haq Khan, A. (2021). Hydrothermally synthesize zinc oxide (ZnO) nanorods as an effective photoanode material for third-generation Dye-sensitized solar cells (DSSCs). *Materials Letters 297*(1), 130017. https://doi.org/10.1016/j.matlet.2021.130017

Supin, K. K., ParvathyNamboothiri, P. M., & Vasundhara, M. (2023). Enhanced photocatalytic activity in ZnO nanoparticles

developed using novel Lepidagathis ananthapuramensis leaf extract. *RSC Advances 13*(3), 1497-1515. https://doi.org/10.1039/D2RA06967A

Taglieri, G., Daniele, V., Maurizio, V., Merlin, G., Siligardi, C., Capron, M., & Mondelli, C. (2023). New eco-friendly and low-energy synthesis to produce ZnO nanoparticles for real-world scale applications. *Nanomaterials 13*(17). https://doi.org/10.3390/nano13172458

Velazquez-Gonzalez, C. E., Armendariz-Mireles, E. N., Pech-Rodriguez, W. J., González-Quijano, D., & Rocha-Rangel, E. (2019). Improvement of dye sensitized solar cell photovoltaic performance by using a ZnO-semiconductor processed by reaction bonded. *Microsystem Technologies 1*(12), 4567-4575. https://doi.org/10.1007/s00542-019-04476-2

Vicencio Garrido, M. A., Portillo Araiza, O. R., Chavez Portillo, M., Portillo, O., & Lozano Espinoza, M. (2023). Crystalline native defects in ZnO analyzed by photoluminescence applying Maxwell-Boltzmann statistics in the visible region. *Revista Mexicana de Física 69*(2 Mar-Apr), 021304 021301-021310. https://doi.org/10.31349/RevMexFis.69.021304

Vivek, S., Preethi, S., & Babu, K. S. (2022). Interfacial effect of mono (Cu, Ni) and bimetallic (Cu-Ni) decorated ZnO nanoparticles on the sunlight assisted photocatalytic activity. *Materials Chemistry and Physics 278*, 125669. https://doi.org/10.1016/j.matchemphys.2021.125669

Wallace, R., Brown, A. P., Brydson, R., Wegner, K., & Milne, S. J. (2013). Synthesis of ZnO nanoparticles by flame spray pyrolysis and characterisation protocol. *Journal of Materials Science 48*(18), 6393-6403. https://doi.org/10.1007/s10853-013-7439-x

Wang, J., Chen, R., Xia, Y., Wang, G., Zhao, H., Xiang, L., & Komarneni, S. (2016). Cost-effective large-scale synthesis of oxygen-defective ZnO photocatalyst with superior activities under UV and visible light. *Ceramics International 43*(1), 1870-1879. https://doi.org/10.1016/j.ceramint.2016.10.146

Wibowo, A., Marsudi, M. A., Amal, M. I., Ananda, M. B., Stephanie, R., Ardy, H., & Diguna, L. J. (2020). ZnO nanostructured materials for emerging solar cell applications. *RSC Advances 10*(70), 42838-42859. doi: 10.1039/D0RA07689A

Yang, X., Deng, Y., Yang, H., Liao, Y., Cheng, X., Zou, Y., . . . Deng, Y. (2023). Functionalization of mesoporous semiconductor metal oxides for gas sensing: Recent advances and emerging challenges. *Advanced Science 10*(1), 2204810. https://doi.org/10.1002/advs.202204810

Yao, N., Huang, J., Fu, K., Deng, X., Ding, M., Shao, M., & Xu, X. (2015). Enhanced light harvesting of dye-sensitized solar cells with up/down conversion materials. *Electrochimica Acta 154*(1), 273-277. https://doi.org/10.1016/j.electacta.2014.12.095

Yousif, Q. A., Mahdi, K. M., & Alshamsi, H. A. (2021). Enhanced photovoltaic performance of dye-sensitized solar cell based on ZnO nanoparticles and ZnO/graphene nanocomposites. *Journal of the Chinese Chemical Society 68*(9), 1637-1643. https://doi.org/10.1002/jccs.202000382

Zapata-Cruz, J. R., Armendáriz-Mireles, E. N., Rocha-Rangel, E., Suarez-Velazquez, G., González-Quijano, D., & Pech-Rodríguez, W. J. (2019). Implementation of Taguchi method to investigate the effect of electrophoretic deposition parameters of SnO_2 on dye sensitised solar cell performance. *Materials Technology 34*(9), 549-557. https://doi.org/10.1080/10667857.2019.1591730

Zatirostami, A. (2021). Fabrication of dye-sensitized solar cells based on the composite TiO_2 nanoparticles/ZnO nanorods: Investigating the role of photoanode porosity. *Materials Today Communications 26*(1), 102033. https://doi.org/10.1016/j.mtcomm.2021.102033